Transmembrane Organization of Yeast Syntaxin-Analogue Sso1p[†]

Yinghui Zhang and Yeon-Kyun Shin*

Department of Biochemistry, Biophysics, and Molecular Biology, Iowa State University, Ames, Iowa 50011

Received October 25, 2005; Revised Manuscript Received February 1, 2006

ABSTRACT: Membrane fusion in secretory pathways is thought to be mediated by SNAREs. It is proposed that membrane fusion transits through hemifusion, a condition in which the outer leaflets of the bilayers are mixed, but the inner leaflets are not. Hemifusion then proceeds to the fusion pore that connects the two internal contents. It is believed that the transmembrane domains (TMDs) of the fusion proteins play an essential role in the transition from hemifusion to the fusion pore. In this work, the structure, dynamics, and membrane topology of the TMD of Sso1p, a target membrane (t-) SNARE involved in the trafficking from Golgi to plasma membrane in yeast, was investigated using site-directed spin labeling and EPR spectroscopy. The EPR analysis of spin-labeled mutants showed that the TMD of Sso1p is a well-defined membrane spanning α-helix. The results also indicate that there is an equilibrium between the monomers and the oligomers. The oligomerization is mainly mediated through the interaction at the *N*-terminal half of the TMD, whereas the *C*-terminal half is free of the tertiary interaction. Additionally, the isotropic hyperfine splitting values were examined for nitroxide-scanning mutants, and it was found that the hyperfine splitting values show a V-shaped profile across the bilayer. Thus, hyperfine splitting may be used as an additional parameter to measure bilayer immersion depths of nitroxide.

Membrane fusion is a widespread process that eukaryotic cells use to establish material transport between endomembrane organelles as well as the secretion from the cell (*1*). In secretory pathways, SNAREs[11] are believed to be core constituents of fusion machinery (*2*−*7*). Vesicle-associated (v-) SNAREs engage with target membrane (t-) SNAREs to form a helical SNARE complex that bridges two membranes (*9*−*14*), facilitating membrane fusion (*6*, *8*). It has been thought that the SNARE complex provides the necessary free energy for membrane fusion (*10*, *15*). However, recent experiments suggest that the SNARE complex acts instead as a catalyst for the fusion of two membranes (*16*, *17*).

SNARE-induced membrane fusion transits through several intermediates (*18*). There is evidence that it proceeds through an intermediate called hemifusion (*19*−*23*), a condition in which the outer leaflets of the two membranes are merged, but the inner leaflets remain intact. In fact, hemifusion has been identified for both class I and class II viral-fusion proteins (*24*−*27*), suggesting that hemifusion might be a common intermediate for many biological fusions (*28*). In the fusion pathway, the hemifusion intermediate subsequently advances to the fusion pore that connects the two aqueous contents (*24*).

Although soluble parts of fusion proteins play a role in bringing about the apposition of two membranes leading to the formation of hemifusion, the transition from hemifusion to the fusion pore requires the transmembrane domain (TMD). For example, when the TMD of SNAREs are shortened or replaced with lipid anchors (*19*, *22*), the fusion process stops at hemifusion, illustrating the role of the TMD in the transition from hemifusion to complete fusion. Similarly, hemifusion has been the final product for modified influenza hemagglutinin (HA) in which the TMD was replaced with a lipid anchor or shortened below the critical length (*29*). Therefore, it may be generally true that the TMDs of fusion proteins play a critical role in promoting the formation of the fusion pore.

In an initial attempt toward understanding of the role of the TMDs in SNARE-mediated membrane fusion, we investigated the structure and dynamics of the TMD of Sso1p, a syntaxin-analogue involved in post-Golgi protein trafficking in yeast, using site-directed spin-labeling EPR (*30*). The results show that the TMD of Sso1p is a transmembrane α-helix with some tilt. Interestingly, there exists an equilibrium between the monomers and the oligomers. Furthermore, the EPR line-shape analysis suggests that the TMD−TMD tertiary contacts are limited in the *N*-terminal half, whereas the *C*-terminal half is free of any tertiary contact.

One of the important parameters of the EPR spectrum is the hyperfine splitting resulting from electron−nucleus dipolar coupling. The hyperfine splitting of a nitroxide is sensitive to the polarity of the environment (*31*) and has been used, for example, as a qualitative indicator of the location

[†] Support for this work was provided by National Institute of Health Grant GM067629.

* To whom correspondence should be addressed. E-Mail: colishin@iastate.edu. Tel: 515-294-2530. Fax: 515-294-0453.

[1] Abbreviations: SNAREs, soluble *N*-ethylmaleimide-sensitive factor attachment protein receptors; EPR, electron paramagnetic resonance; TMD, transmembrane domain; v-, vesicle-associated; t-, target membrane; POPC, 1-palmitoyl-2-dioleoyl-sn-glycero-3-phosphatidylcholine; DOPS, 1,2-dioleoyl-sn-glycero-3-phosphatidylserine; MTSSL, methanethiosulfonate spin label; IPTG, isopropyl-*β*-D-thiogalactopyranoside; LB, Luria-B broth; PBST, phosphate-buffered saline at pH 7.4 with 0.5% Triton X-100 (v/v); NiEDDA, nickel ethylenediaminediacetic acid; GST, glutathione *S*-transferase; AEBSF, 4-(2-aminoethyl)benzenesulfonyl fluoride; DTT, dithiothreitol.

10.1021/bi052178+ CCC: $33.50
Published on Web 03/09/2006

of nitroxide in the membrane environment (*33*−*35*). Because the TMD of Sso1p is now shown to be a well-defined membrane-spanning α-helix, its nitroxide-scanning mutants may serve as an ideal model system to examine the variation of hyperfine splitting across the bilayer. The plot of isotropic hyperfine splitting versus the residue number shows a symmetric V-shaped curve, which may be used as a calibration curve to estimate the immersion depth of nitroxide in the membrane.

EXPERIMENTAL PROCEDURES

Plasmid Construction and Site-directed Mutagenesis. The DNA sequence encoding Sso1pHT (amino acids 185−290 of Sso1p) was inserted into the pGEX-KG vector between EcoRI and HindIII sites as *N*-terminal glutathione *S*-transferase (GST) fusion proteins (*16*). To introduce a unique cysteine residue for the specific nitroxide attachment, native cysteine 266 of Sso1pHT was mutated to alanine. A QuickChange site-directed mutagenesis kit (Stratagene) was used to generate all mutants; DNA sequences were confirmed by the Iowa State University DNA sequencing facility.

Protein Expression, Purification, and Spin Labeling. The expression of recombinant GST fusion proteins was conducted in *E. coli* Rosetta (DE3) pLysS (Novagene). The cells were grown at 37 °C in an LB medium with glucose (2 g/L), ampicillin (100 μg/mL), and chloramphenicol (25 μg/mL) until the A_{600} value reached 0.6−0.8. Isopropyl-β-D-thiogalactopyranoside (IPTG) was added to a final concentration of 1 mM. The cells were grown for four more hours at 18 °C. The cell pellets were harvested by centrifugation at 6000 rpm for 10 min.

Purification of GST fusion proteins was achieved with affinity chromatography using glutathione-agarose beads (Sigma). Frozen cell pellets were resuspended in a PBS buffer (phosphate-buffered saline at pH 7.4 with 0.5% Triton X-100 (v/v), PBST) with 2 mM 4-(2-aminoethyl)benzenesulfonyl fluoride (AEBSF) and 5 mM dithiothreitol (DTT). The cells were broken by sonication in an ice bath. As for Sso1pHT, 1% of *n*-lauroyl sarcosine was added to the solution before sonication. The cell lysate was centrifuged at 15 000*g* for 20 min at 4 °C. The supernatant was mixed with glutathione-agarose beads in the resuspension buffer and nutated at 4 °C for 120 min. The protein-bound beads were washed with an excess volume of washing buffer (phosphate-buffered saline at pH 7.4) for at least six rounds. When washing, 0.2% (v/v) Triton X-100 was added to Sso1pHT. The beads were then washed with a thrombin-cleavage buffer (50 mM Tris-HCl, 150 mM NaCl, and 2.5 mM $CaCl_2$ at pH 8.0) and 0.2% Triton X-100. Finally, the proteins were cleaved from the resin by thrombin (Sigma) at room temperature for 40 min. AEBSF was added to the protein after cleavage (2 mM final concentration) to inhibit continuous cleavage by thrombin. The protein was stored at −80 °C with 10% glycerol.

Cysteine mutants of Sso1pHT were spin labeled before thrombin cleavage. After the cell lysate was incubated with beads and washed with the PBS buffer containing 0.2% Triton X-100, DTT was added to a final concentration of 5 mM. The sample was incubated at 4 °C for 40 min, and the beads were then washed six times with an excess volume of the PBS buffer with 0.2% Triton X-100 to remove DTT. About 20-fold excess of (1-oxyl-2,2,5,5-tetramethylpyrrolinyl-3-methyl) methanethiosulfonate spin label (MTSSL) was immediately added to the protein. The reaction mixture was left overnight at 4 °C. Free MTSSL was removed by washing with excess PBS buffer with 0.2% Triton X-100. The proteins were cleaved by thrombin in a cleavage buffer with 0.2% Triton X-100. Thrombin was not removed from the protein samples. It was expected that the small amount of thrombin (3 μM) would not influence the experimental data.

Membrane Reconstitution. Large unilamellar vesicles (∼100 nm in diameter) of 1-palmitoyl-2-dioleoyl-sn-glycero-3-phosphatidylcholine (POPC) containing 15% 1,2-dioleoyl-sn-glycero-3-phosphatidylserine (DOPS) were prepared in a detergent-free cleavage buffer using an extruder (*36*). The total lipid concentration was 100 mM. The proteins were reconstituted into vesicles by the Bio-Beads method (*36*): The proteins were mixed with vesicles at a ∼1:300 protein-to-lipid molar ratio. The detergent was removed by treating the sample with Bio-beads SM2 (Bio-rad), which was directly added to the sample in the ratio of 200 mg/1 mL of the mixed solution. After 45 min of nutation, the Bio-beads were removed from the sample by centrifugation at 10 000*g* for 1 min. The same procedure was repeated three times. Reconstitution efficiency was estimated by determining the protein concentration using EPR before and after reconstitution. For all samples, the efficiency was approximately 70%. To determine the orientation of reconstituted Sso1pHT on the vesicle, we treated the reconstituted protein with 2 mM trypsin for 1 h. An SDS−PAGE analysis indicated that the Sso1pHT protein was almost completely digested to small fragments (data not shown), suggesting that a majority of Sso1pHT analogues were oriented toward the outside of the vesicle.

EPR Experiments and Analysis. EPR spectra were obtained with a Bruker ESP 300 EPR spectrometer equipped with a loop-gap resonator. The modulation amplitude was set at no greater than one-fourth of the line width. Spectra were collected at either room temperature or 130 K in the first-derivative mode. At room temperature, the microwave power was kept at 1 mW, but it was set at 8 μW at 130 K to avoid the saturation of EPR lines. All protein samples contained 10−15% glycerol as a cryoprotectant. For low-temperature EPR, the capillary sample tubes were plunged quickly into liquid nitrogen for fast freezing.

For saturation EPR, the gas exchange to the protein sample was achieved with a TPX tube for the loop-gap resonator. For individual mutants, power saturation curves were obtained from the peak-to-peak amplitude of the central line ($M_I = 0$) of the first-derivative EPR spectrum as a function of incident microwave power in the range of 0.1−40 mW. Three power saturation curves were obtained for each mutant after equilibration with (1) N_2, (2) air (O_2), and (3) N_2 in the presence of 200 mM NiEDDA (nickel ethylenediaminediacetic acid). From the saturation curves, the microwave power $P_{1/2}$ (mW) where the first-derivative amplitude is reduced to one-half of its unsaturated value was calculated. The quantity $\Delta P_{1/2}$ is the difference in $P_{1/2}$ values in the presence and absence of a paramagnetic reagent, which is proportional to the diffusion coefficient times the frequency of the collision of nitroxide with freely diffusing reagents such as oxygen and NiEDDA. Thus, $\Delta P_{1/2}$ is considered to be equivalent to the accessibility *W*. The immersion depth

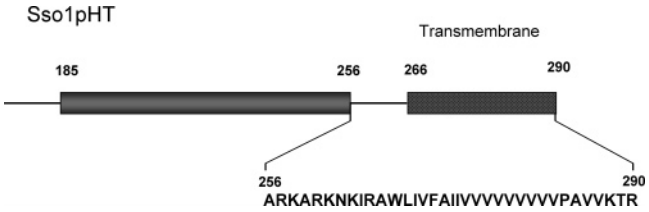

FIGURE 1: Primary structure of yeast Sso1pHT. Sso1pHT contains Sso1p amino acids 185−290. This polypeptide includes both the SNARE motif and the transmembrane domain, which are represented by a cylinder and a rectangle, respectively. Between them is the linker region that contains amino acids 256−265. The spin-labeled positions are shown below the schematic diagram.

is calculated on the basis of the reference curves determined from a set of lipid molecules spin-labeled at different acyl chain positions (*40*).

The isotropic hyperfine splitting for each spin-labeled mutant was determined empirically by measuring the peak-to-peak separation between the first and center lines of the EPR spectrum. This empirical value should be considered as an approximate measure of isotropic hyperfine splitting. It is expected that isotropic hyperfine splitting is independent of motional broadening or inhomogeneous line broadening as long as the molecules are not macroscopically oriented.

RESULTS

Site-Directed Spin-Labeling EPR for the TMD of Yeast t-SNARE Sso1p. To investigate the transmembrane structure of yeast t-SNARE Sso1p using EPR, native residues were replaced one by one with cysteines that were modified with a nitroxide spin label. The Sso1pHT used in this study consisted of amino acids 185−290 of Sso1p without the *N*-terminal regulatory Habc domain. We made 35 single-cysteine mutants of Sso1pHT ranging from a.a. 256 through 290, which include the putative linker region (a.a. 256−265) and the putative TMD region (a.a. 266−280) (Figure 1). The spin labeling efficiency was greater than 80% for all mutants. Each spin-labeled mutant was reconstituted into the vesicles made of 1-palmitoyl-2-dioleoyl-sn-glycero-3-phosphatidylcholine (POPC) and 1,2-dioleoyl-sn-glycero-3-phosphatidylserine (DOPS) (molar ratio of 85:15), lipids commonly used for in vitro studies of SNARE proteins. The functionality of the spin-labeled Sso1pHT mutants was tested using an in vitro fluorescence-fusion assay (*36*). All mutants showed at least 57% of the fusion activity of wild-type Sso1pHT (Figure 2).

After the reconstitution of Sso1pHT mutants into phospholipid vesicles, the EPR spectra were collected for spin-labeled mutants at room temperature (Figure 3). For A256C−A259C, the EPR spectra are composed of two components, one sharp (arrow) and the other relatively broad (asterisk). Because these positions are located near the water−membrane interface, we expect that the region might be in equilibrium between the free and membrane-bound states. Thus, it is likely that the sharp component represents the subpopulation that is free in solution, whereas the broad component represents the subpopulation that interacts with the membrane surface and tumbles slowly in the viscous headgroup region.

EPR spectra for R260C to A266C are all broad, indicating that the region is fully inserted into the membrane. The extent of line broadening in this region is prototypical for the

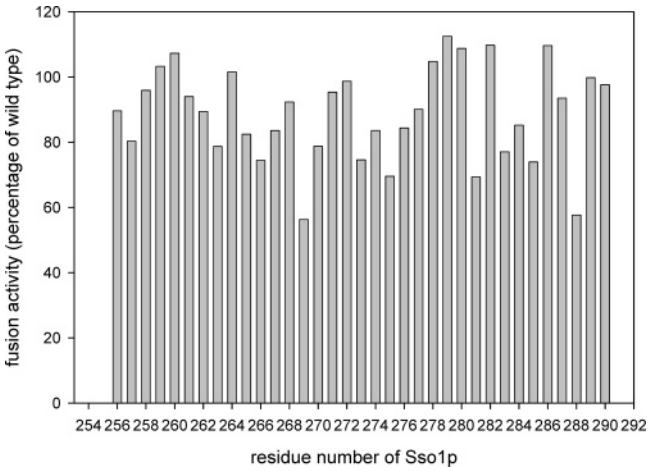

FIGURE 2: Fusion activity of spin-labeled Sso1pHT mutants**.** The fusion activity of each spin-labeled Sso1pHT mutant was measured using an in vitro fusion assay. The percent fusion activity of the mutant was calculated in reference to the fusion activity of the wild type.

nitroxide embedded in the headgroup region of the bilayer (*37*, *38*) except for K261C, where we observed an extensive line broadening perhaps due to the tertiary interaction with the neighboring molecules. The EPR spectra for W267C and L268C are slightly narrower than those of the preceding positions, suggesting that residues following position 267 enter into the less viscous acyl chain region. Among those, positions 269, 270, 272, 273, and 276 manifest broad spectral components, indicative of tertiary contacts most likely with the neighboring TMDs. Importantly, the presence of two spectral components suggests that there may be equilibrium between the monomeric TMD and the oligomeric TMDs. We note that the five interacting positions reside within the *N*-terminal half of the TMD, revealing that the TMD−TMD interaction is mostly confined within the *N*-terminal half of the TMD.

The inverse of the central line width is often used as a semiquantitative measure of the tumbling rates of nitroxide (*39*). The line-shape parameter is plotted as a function of the residue number in Figure 4. In this Figure, it is clearly demonstrated that residue 259 is located right at the water−headgroup boundary. The line-shape parameter for residues from 260 to 276 remained near 0.24, although there are some variations along the sequence. However, we observe a significant and gradual increase in the lower half of the TMD, indicative of the increased dynamics at the *C*-terminal half of the Sso1pHT TMD.

Transmembrane Structure of Sso1pHT TMD Determined by Accessibility Measurements. We then investigated the nitroxide-scanning mutants of Sso1pHT using the EPR saturation method to determine the topology of the Sso1pHT TMD in the membrane (*36*, *40*). With this EPR method, we measured the accessibility of nitroxide to a water-soluble paramagnetic reagent, nickel-ethylenediaminediacetic acid (NiEDDA) (W_{NiEDDA}), to estimate the extent of the seclusion of the spin-labeled site from the aqueous phase. We also measured the accessibility of the nitroxide to a nonpolar paramagnetic reagent, molecular oxygen (W_{O_2}), to probe the immersion into the nonpolar membrane interior.

In Figure 5a, the W_{NiEDDA} and W_{O_2} values for the spin-labeled mutants of Sso1pHT are plotted as functions of the

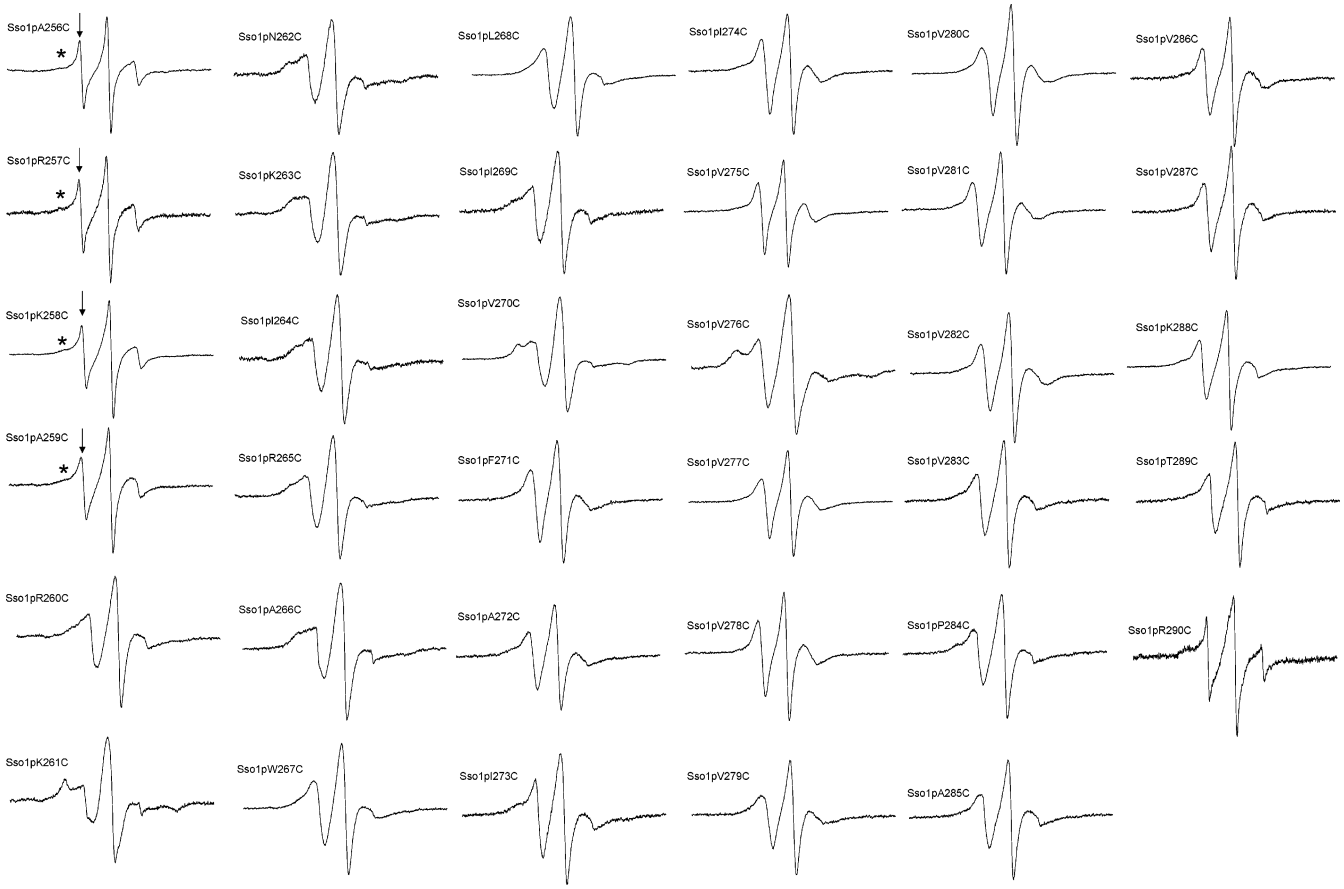

FIGURE 3: Room-temperature EPR spectra of spin-labeled Sso1pHT transmembrane mutants**.** The EPR spectra for A256C−A259C are composed of two spectral components: one sharp (arrows) and the other, relatively broad (asterisks).

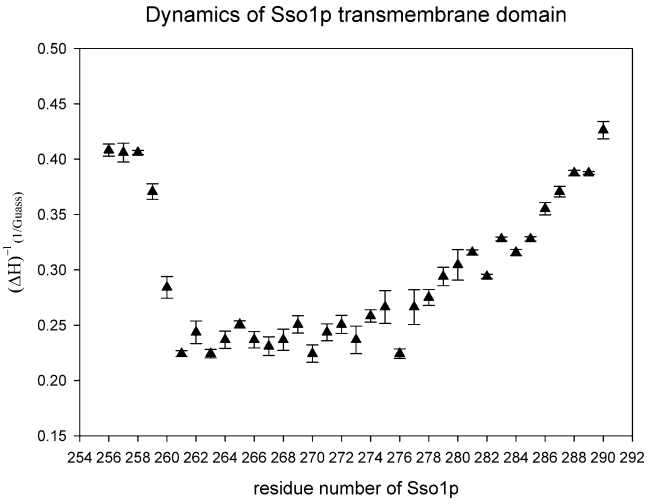

FIGURE 4: Dynamic profile across the Sso1pHT TMD. The inverse line width $(\Delta H)^{-1}$, which reflects the motion of the nitroxide, is plotted as a function of the residue number with arbitrary units. The inverse line width was calculated from the peak-to-peak width of the central line. The high $(\Delta H)^{-1}$ value reflects the fast motion and the low $(\Delta H)^{-1}$ value reflects the slow motion. The error bar represents the standard deviation of the results from three independent measurements of line width.

residue number. The W_{NiEDDA} values show the representative U-shaped curve expected for a polypeptide passing through the entire bilayer. The collision with NiEDDA starts with very high values, indicative of the solvent exposure of the first few residues. The valley of low-collision frequency in the middle reflects the passage of the peptide chain through the bilayer. The collision frequency increases again to high values, showing the re-emergence of the peptide chain to the solution phase. In contrast, the collision with oxygen is inversely correlated with the behavior of the collision with NiEDDA; when the W_{NiEDDA} values are low, the Wo_2 values are high and vice versa. Such an inverse correlation of W_{NiEDDA} and Wo_2 has been considered as strong evidence of the membrane-spanning peptide. Over the entire range, the W_{NiEDDA} profile and the W_{O2} profile crisscross each other twice, once near positions 263−265 and again near position 284.

For I269C, I273C, and V276C, the Wo_2 values are noticeably lower than those of other membrane-spanning residues. It is important to note that these three positions belong to the group of residues that show a broad spectral component stemming from tertiary contacts. In the helical wheel diagram (Figure 5c), these positions (color coded in red) are lined on one side of the helical surface, revealing the interacting surface of Sso1pHT TMD.

Quantitatively, it has been shown that the immersion depth of nitroxide is proportional to the logarithm of the ratio of W_{NiEDDA} to Wo_2. For individual positions, the immersion depths were calculated by comparing the ratios of W_{NiEDDA} to Wo_2 to a standard curve (*40*, *41*) and the results were plotted with respect to residue numbers in Figure 5b. As expected, we obtained an overall V-shaped curve with the lowest point at position 275, which is located approximately 19 Å from the phosphate group near the center of the bilayer. It was also evident that residues 262−264 reside near the boundary between the headgroup region and the acyl chain

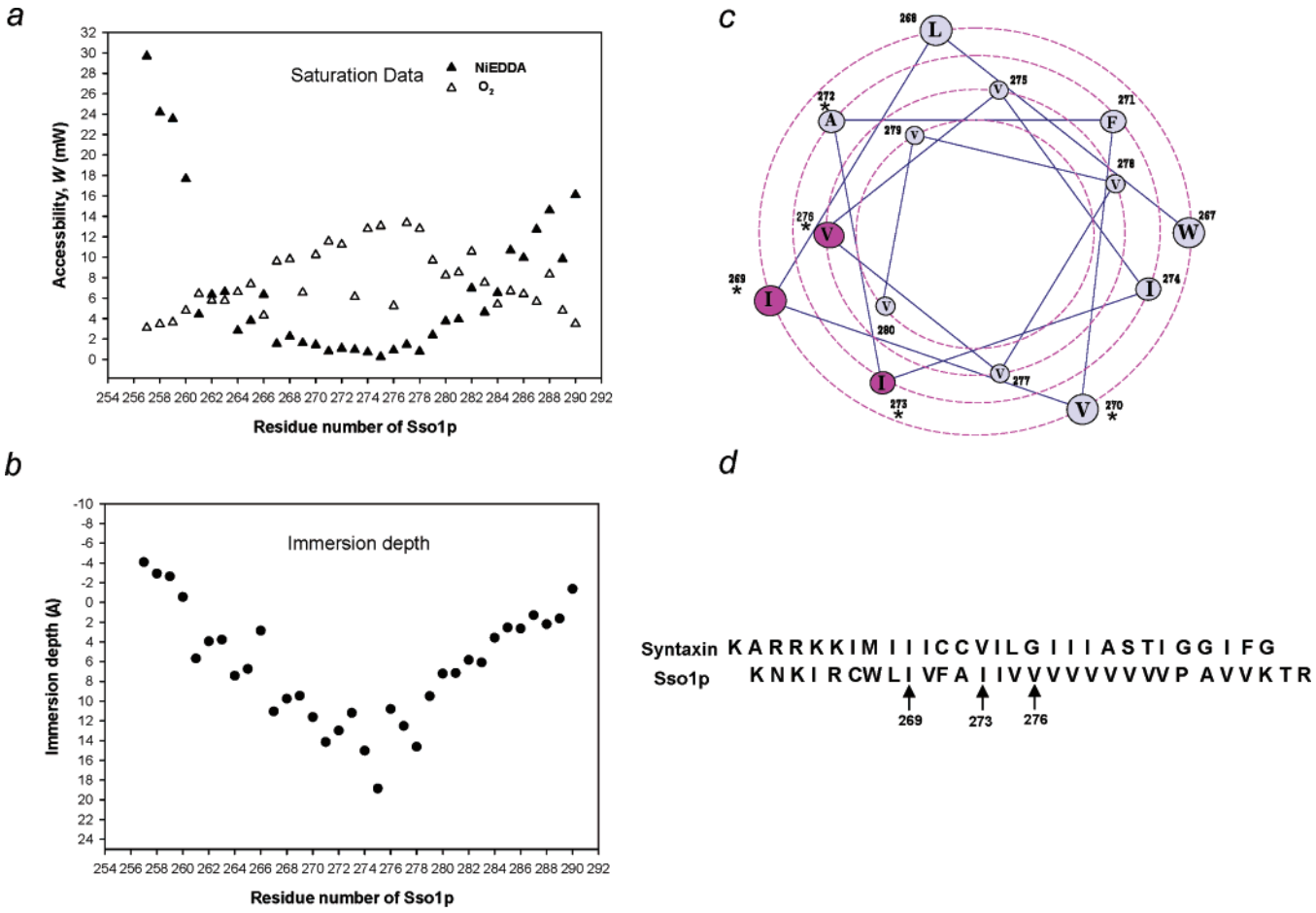

FIGURE 5: Structural determination of the Sso1pHT transmembrane domain with EPR accessibility measurements. (a) Accessibility parameters W_{O2} (△) and W_{NiEDDA} (▲) are plotted as functions of the residue number. (b) Membrane immersion depths vs the residue number. (c) A helical wheel diagram for the Sso1pHT TMD. Positions 269, 270, 272, 273, and 276, which show the tertiary contacts in the EPR spectra, are marked with asterisks, whereas positions 269, 273, and 276, which show the reduced W_{O2} values, are color coded in red. (d) Sequence alignment between the TMDs of neuronal syntaxin and Sso1p. Positions 269, 273, and 276, which show the tertiary interaction in this work, match one-to-one to the proposed pore-lining positions in syntaxin.

region, which is located approximately 6 Å below the phosphate group (0 Å). On the other side of the membrane, residue 284 (proline) sits at the headgroup−acyl chain boundary. Therefore, from the immersion depth data, it appears that approximately 21 residues (from residue 264 to residue 284) span the 27−30 Å thick acyl chain region. Considering the geometry of a standard α-helix (1.5 Å/residue), this result supports the idea that the TMD is a membrane-spanning α-helix with some tilt with respect to the membrane normal. The tilt angle was estimated to be less than 30°, although the exact value was difficult to determine. Furthermore, it is interesting to find that the data appears more scattered in the *N*-terminal half of the TMD than it does in the *C*-terminal half. This is likely due to the TMD−TMD interactions in the *N*-terminal half because the tertiary interaction at several residues makes accessibility measurements uncertain and leads to larger errors.

Low-Temperature EPR to Measure Interspin Distances. The EPR line-shape analysis indicated that residues 269, 270, 272, 273, and 276 might have partial tertiary contacts with neighboring TMDs; the EPR spectra are composed of two spectral components, indicating that there might be equilibrium between the monomeric TMD and multimeric TMDs. The Fourier deconvolution method (*42*) has proven to be powerful in determining the interspin distance between two interacting nitroxides and in estimating the percentage of the interacting spins when there is equilibrium between the interacting population and the noninteracting population (*43*). The low-temperature EPR spectra taken at 130 K (Figure 6, left panel) showed the line broadening due to the spin−spin interaction for all positions except position 270. The Fourier spectral analysis revealed that the monomer fraction consists of 60, 66, 56, and 68% for positions 269, 272, 273, and 276, respectively; Figure 6, right panel). The interspin distances in the oligomeric state were estimated by analyzing the remaining interacting factions, and they were 12−13 Å for all four positions. Thus, the Fourier deconvolution method strongly supports the idea that residues 269, 272, 273, and 276 participate in the intermolecular interaction between the TMDs. Position 270 is likely to be a peripheral residue for which the distance between residues is larger than 25 Å.

To verify the equilibrium between the monomeric TMD and the multimeric TMDs, we collected room-temperature EPR spectra for residue 273 at three different concentrations (Figure 7). We found that the broad spectral component (arrows in Figure 7), reflecting the oligomeric TMDs, increased noticeably as the protein concentration was increased, strongly supporting the idea that the monomers and multimers are in equilibrium.

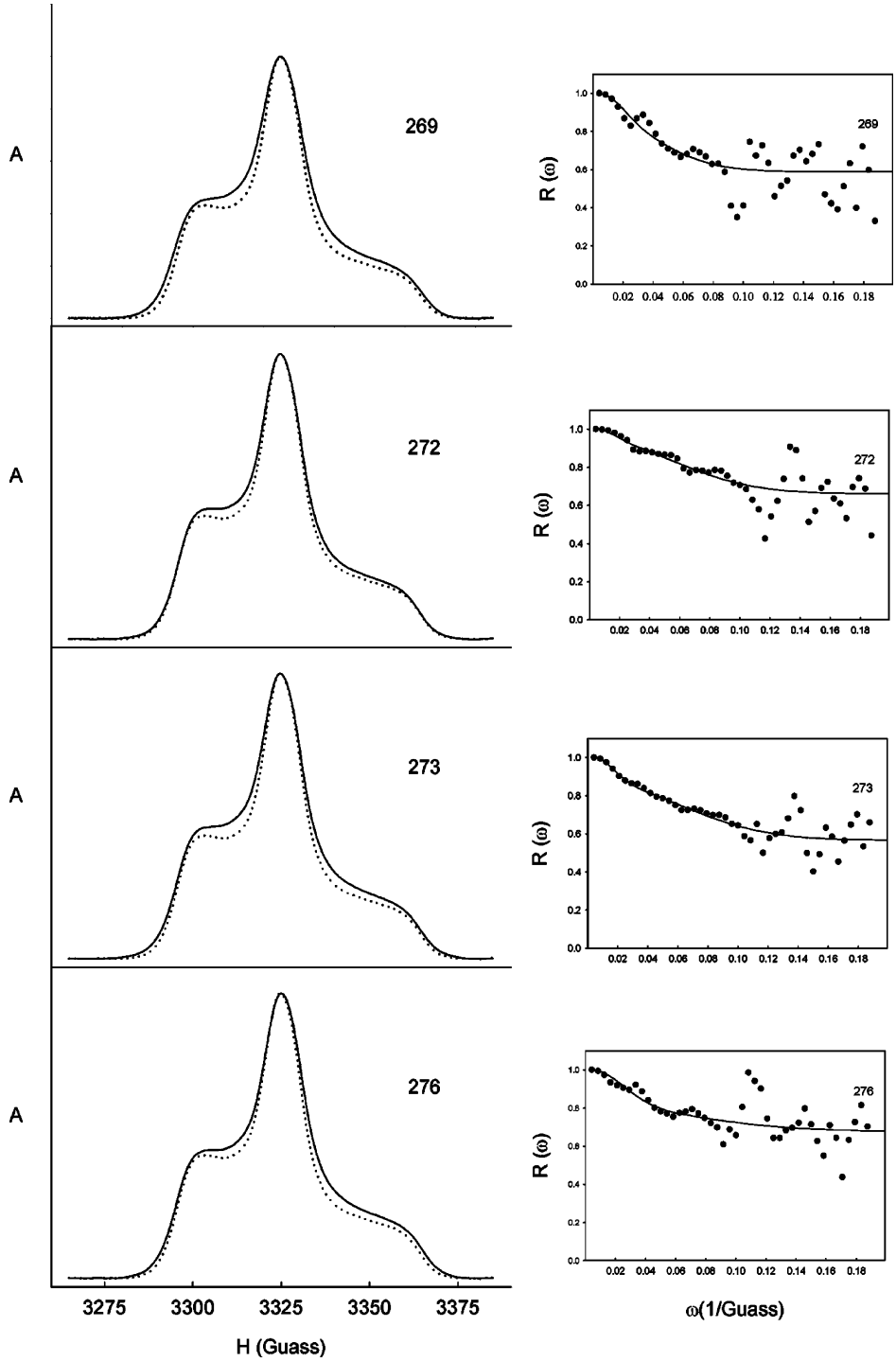

FIGURE 6: Low-temperature EPR spectra and Fourier deconvolution analysis for spin labeled Sso1pHT. Low-temperature absorbance (integrated) spectra for spin-labeled mutants (—) were compared with a noninteracting reference spectrum (....) in the left panel. The dipolar broadening functions (in Fourier space) are shown in the right panel. The data was fitted with a sum of two Gaussians (—). In the Fourier space, the fraction of noninteracting monomers appears as a constant *y*-axis offset (*42*, *43*). The *y*-axis offsets were around 60%.

Isotropic Hyperfine Splitting Reflects the Membrane Immersion Depths. One of the important parameters of the EPR spectrum is the hyperfine splitting resulting from electron−nucleus dipolar coupling. The hyperfine splitting of a nitroxide is sensitive to the polarity of the environment and has been used as a means to measure the partitioning of a small nitroxide between water and the membrane, which has been used to detect the bilayer phase transition (*32*). Furthermore, this parameter has also been used as a qualitative indicator of the location of the nitroxide in the membrane environment (*33*, *34*, *35*, *44*). Because the detailed structural features of the Sso1pHT TMD are now determined, the isotropic hyperfine values of the Sso1pHT mutants can serve as a model to explore the relationship between the hyperfine splitting profile across the bilayer and the membrane immersion depth. We attempted to plot the isotropic hyperfine splitting values of individual positions along the sequence (Figure 8). The plot shows an overall V-shaped curve; higher hyperfine splitting value as the positions move away from the center of the bilayer. Interestingly, the curve is symmetric and linear in the range of a.a. 266−284 which form the core helix spanning the acyl chain region of the bilayer. Near the

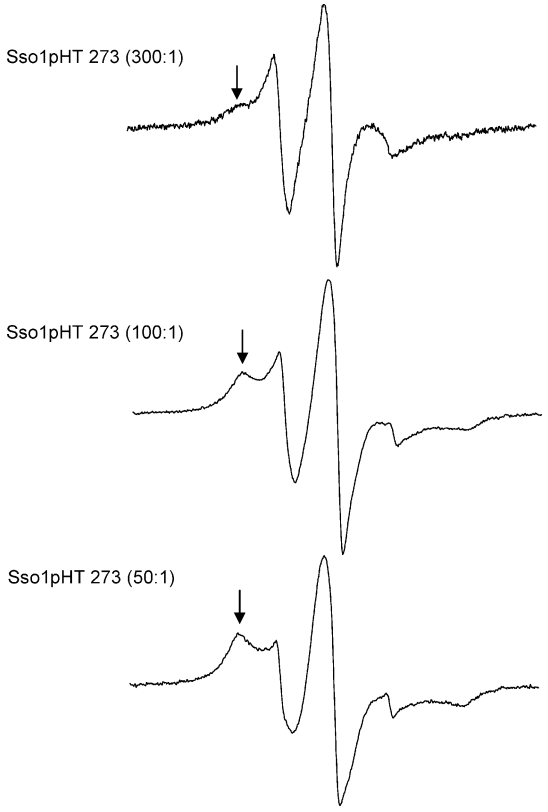

FIGURE 7: Room-temperature EPR spectra of spin-labeled Sso1pHT mutant I273C**.** The molar lipid-to-protein ratios are given in parentheses. The arrows indicate the broad spectral component reflecting the multimers.

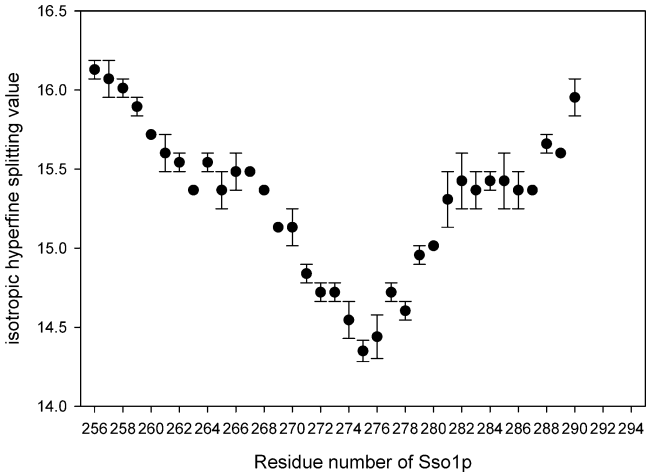

FIGURE 8: Profile of isotropic hyperfine splitting across the bilayer for the Sso1pHT TMD. Isotropic hyperfine splitting for each spin-labeled mutant was determined by measuring the peak-to-peak separation between the first and center lines of the EPR spectrum. The error bars represent the standard deviation of results from three independent isotropic hyperfine-splitting analyses.

headgroup−acyl chain interface, the curve shows discontinuities: one on the *N*-terminal side (a.a. 263−265) and another near residue 284 on the *C*-terminal side. The discontinuity at the *N*-terminal side might indicate that this region might not exist as an α-helix, consistent with previous results for syntaxin (*38*). However, we note that residue 284 is proline, which is a known helix breaker. Therefore, the break in the profile near position 284 may be attributed to the discontinuity in the α-helix structure near the headgroup−acyl chain interface. The results suggest that hyperfine splitting can be used as a complimentary measure of the membrane immersion depth of nitroxide for membrane-embedded helices.

DISCUSSION

The EPR analysis of spin-labeled mutants suggests that the TMDs of Sso1pHT have a tendency to interact with one another, most likely to form an oligomeric structure. The results also show that there may be an equilibrium between the monomeric form and the oligomeric forms in a molar ratio of approximately 6:4 at the lipid-to-protein ratio of 300:1. Interestingly, the EPR line shapes showed that the tertiary contacts are limited within the *N*-terminal half, whereas the *C*-terminal half is free of such interactions. This result is consistent with the significant increase in the motional dynamics in the *C*-terminal region of the TMD (Figure 4). Potentially, the interaction between the TMDs would help the oligomerization of the SNARE complex at the fusion site. The oligomerization of the neuronal counterpart syntaxin has also been reported (*45*−*47*).

Combining the EPR line-shape analysis, accessibility measurements, and the Fourier-deconvolution analysis, it seems that residues 269, 273, and 276 are the positions involved in the tertiary interactions when the TMDs of Sso1pHT gather together. These residues are located on one side of the helix and form a well-defined interacting surface (see the helical wheel diagram in Figure 5c). Interestingly, the sequence alignment between neuronal syntaxin and yeast Sso1pHT (Figure 5d) reveals that residues 269, 273, and 276 match one-to-one to the residues in syntaxin that are proposed to line the transmembrane pore (*48*).

Oligomerization appears to be generally required for a variety of fusion proteins. For SNAREs, it has been shown that the coordination of at least three SNARE complexes is necessary for successful fusion (*49*). For influenza hemagglutinin (HA), it appears that 4−6 HA molecules work together at the fusion site (*50*). On the basis of electrical measurements, it has been proposed that 5−8 syntaxin TMDs form a cluster (*48*). In contrast, it has been previously shown that syntaxin forms dimers in the membrane (*38*). In the present EPR, it was not possible to estimate the exact stoichiometry of the oligomeric Sso1pHT TMDs, although partial clustering is clearly demonstrated.

Over the last several years, the EPR saturation method has proven powerful in determining the structure and topology of membrane-bound peptides and proteins. Although isotropic hyperfine splitting has often been used qualitatively to verify membrane insertion of polypeptides, its entire profile across the membrane was not extensively investigated. The TMD of Sso1pHT is a well-defined transmembrane helix and has served as an excellent system to determine the full profile of hyperfine splitting. The clean profile in Figure 8 demonstrates that a simple measurement of isotropic hyperfine splitting may be useful in assessing the immersion depths of nitroxides, in addition to the results from a well-established EPR saturation method.

REFERENCES

1. Earp, L. J., Delos, S. E., Park, H. E., and White, J. M. (2005) The many mechanisms of viral membrane fusion proteins, *Curr. Top. Microbiol. Immunol. 285*, 25−66.

2. Rothman, J. E. (1994) Mechanisms of intracellular protein transport, *Nature 372*, 55−63.
3. Chen, Y. A., Scales, S. J., Patel, S. M., Doung, Y. C., and Scheller, R. H. (1999) SNARE complex formation is triggered by Ca2+ and drives membrane fusion, *Cell 97*, 165−174.
4. Rothman, J. E. (2002) The machinery and principles of vesicle transport in the cell, *Nat. Med. 8*, 1059−1062.
5. Sollner, T., Bennett, M. K., Whiteheart, S. W., Scheller, R. H., and Rothman, J. E. (1993) A protein assembly-disassembly pathway in vitro that may correspond to sequential steps of synaptic vesicle docking, activation, and fusion, *Cell 75*, 409−418.
6. McNew, J. A., Parlati, F., Fukuda, R., Johnston, R. J., Paz, K., Paumet, F., Sollner, T. H., and Rothman, J. E. (2000) Compartmental specificity of cellular membrane fusion encoded in SNARE proteins, *Nature 407*, 153−159.
7. Jahn, R., Lang, T., and Sudhof, T. C. (2003) Membrane fusion, *Cell 112*, 519−533.
8. Weber, T., Zemelman, B. V., McNew, J. A., Westermann, B., Gmachl, M., Parlati, F., Sollner, T. H., and Rothman, J. E. (1998) SNAREpins: Minimal machinery for membrane fusion, *Cell 92*, 759−772.
9. Poirier, M. A., Xiao, W., Macosko, J. C., Chan, C., Shin, Y. K., and Bennett, M. K. (1998) The synaptic SNARE complex is a parallel four-stranded helical bundle, *Nat. Struct. Biol. 5*, 765−769.
10. Sutton, R. B., Fasshauer, D., Jahn, R., and Brunger, A. T. (1998) Crystal structure of a SNARE complex involved in synaptic exocytosis at 2.4 Å resolution, *Nature 395*, 347−353.
11. Hanson, P. I., Roth, R., Morisaki, H., Jahn, R., and Heuser, J. E. (1997) Structure and conformational changes in NSF and its membrane receptor complexes visualized by quick-freeze/deep-etch electron microscopy, *Cell 90*, 523−535.
12. Lin, R. C., and Scheller, R. H. (1997) Structural organization of the synaptic exocytosis core complex, *Neuron 19*, 1087−1094.
13. Katz, L., Hanson, P. I., Heuser, J. E., and Brennwald, P. (1998) Genetic and morphological analyses reveal a critical interaction between the C-termini of two SNARE proteins and a parallel four helical arrangement for the exocytic SNARE complex, *EMBO J. 17*, 6200−6209.
14. Antonin, W., Fasshauer, D., Becker, S., Jahn, R., and Schneider, T. R. (2002) Crystal structure of the endosomal SNARE complex reveals common structural principles of all SNAREs, *Nat. Struct. Biol. 9*, 107−111.
15. Kweon, D. H., Kim, C. S., and Shin, Y. K. (2003) Insertion of the membrane-proximal region of the neuronal SNARE coiled coil into the membrane, *J. Biol. Chem. 278*, 12367−12373.
16. Zhang, Y., Su, Z., Zhang, F., Chen, Y., and Shin, Y. K. (2005) A partially zipped SNARE complex stabilized by the membrane, *J. Biol. Chem. 280*, 15595−15600.
17. Chen, Y. A., Scales, S. J., Jagath, J. R., and Scheller, R. H. (2001) A discontinuous SNAP-25 C-terminal coil supports exocytosis, *J. Biol. Chem. 276*, 28503−28508.
18. Ungermann, C., and Langosch, D. (2005) Functions of SNAREs in intracellular membrane fusion and lipid bilayer mixing, *J. Cell Sci. 118*, 3819−3828.
19. Xu, Y., Zhang, F., Su, Z., Mcnew, J. A., and Shin, Y. K. (2005) Hemifusion in SNARE-mediated membrane fusion, *Nat. Struct. Mol. Biol. 12*, 417−422.
20. Reese, C., Heise, F., and Mayer, A. (2005) Trans-SNARE pairing can precede a hemifusion intermediate in intracellular membrane fusion, *Nature 436*, 410−414.
21. Lu, X., Zhang, F., McNew, J. A., and Shin, Y. K. (2005) Membrane fusion induced by neuronal SNAREs transits through hemifusion, *J. Biol. Chem. 280*, 30538−30541.
22. Giraudo, C. G., Hu, C., You, D., Slovic, A. M., Mosharov, E. V., Sulzer, D., Melia, T. J., and Rothman, J. E. (2005) SNAREs can promote complete fusion and hemifusion as alternative outcomes, *J. Cell Biol. 170*, 249−260.
23. Chernomordik, L. V., Vogel, S. S., Sokoloff, A., Onaran, H. O., Leikina, E. A., and Zimmerberg, J. (1993) Lysolipids reversibly inhibit Ca(2+)-, GTP- and pH-dependent fusion of biological membranes, *FEBS Lett. 318*, 71−76.
24. Chernomordik, L. V., and Kozlov, M. M. (2003) Protein-lipid interplay in fusion and fission of biological membranes, *Annu. Rev. Biochem. 72*, 175−207.
25. Zaitseva, E., Mittal, A., Griffin, D. E., and Chernomordik, L. V. (2005) Class II fusion protein of alphaviruses drives membrane fusion through the same pathway as class I proteins, *J. Cell Biol. 169*, 167−177.
26. Kemble, G. W., Danieli, T., and White, J. M. (1994) Lipid-anchored influenza hemagglutinin promotes hemifusion, not complete fusion, *Cell 76*, 383−391.
27. Melikyan, G. B., Markosyan, R. M., Roth, M. G., and Cohen, F. S. (2000) A point mutation in the transmembrane domain of the hemagglutinin of influenza virus stabilizes a hemifusion intermediate that can transit to fusion, *Mol. Biol. Cell 11*, 3765−3775.
28. White, J. M., and Castle, J. D. (2005) Searching for the silver lining, *Nat. Struct. Mol. Biol. 12*, 382−384
29. Armstrong, R., T., Kushnir, A. S., and White, J. M. (2000) The transmembrane domain of influenza hemagglutinin exhibits a stringent length requirement to support the hemifusion to fusion transition, *J. Cell Biol. 151*, 425−437.
30. Hubbell, W. L., Gross, A., Langen, R., and Lietzow, M. A. (1998) Recent advances in site-directed spin labeling of proteins, *Curr. Opin. Struct. Biol. 8*, 649−656.
31. Seelig, J., and Hasselbach, W. (1971) A spin label study of sarcoplasmic vesicles, *Eur. J. Biochem. 21*, 17−21.
32. Shimshick, E. J., and McConnell, H. M. (1973) Lateral phase separation in phospholipid membranes, *Biochemistry 12*, 2351−2360.
33. Shin, Y. K., Levinthal, C., Levinthal, F., and Hubbell, W. L. (1993) Colicin E1 binding to membranes: time-resolved studies of spin-labeled mutants, *Science 259*, 960−963.
34. Yu, Y. G., King, D. S., and Shin, Y. K. (1994) Insertion of a coiled-coil peptide from influenza virus hemagglutinin into membranes, *Science 266*, 234−236.
35. Gross, A., Columbus, L., Hideg, K., Altenbach, C., and Hubbell, W. L. (1999) Structure of the KcsA potassium channel from *Streptomyces lividans*: a site-directed spin labeling study of the second transmembrane segment, *Biochemistry 38*, 10324−10335.
36. Chen, Y., Xu, Y., Zhang, F., and Shin, Y. K. (2004) Constitutive versus regulated SNARE assembly: a structural basis, *EMBO J. 23*, 681−689.
37. Kweon, D. K., Kim, C. S., and Shin, Y. K. (2002) The membrane-dipped neuronal SNARE complex: a site-directed spin labeling electron paramagnetic resonance study, *Biochemistry 41*, 9264−9268.
38. Kim, C. S., Kweon, D. K., and Shin, Y. K. (2002) Membrane topologies of neuronal SNARE folding intermediates, *Biochemistry 41*, 10928−10933.
39. Kweon, D. H., Kim, C. S., and Shin, Y. K. (2003) Regulation of neuronal SNARE assembly by the membrane, *Nat. Struct. Biol. 10*, 440−447.
40. Altenbach, C., Greenhalgh, D. A., Khorana, H. G., and Hubbell, W. L. (1994) A collision gradient method to determine the immersion depth of nitroxides in lipid bilayers: application to spin-labeled mutants of bacteriorhodopsin, *Proc. Natl. Acad. Sci. U.S.A. 91*, 1667−1671.
41. Macosko, J. C., Kim, C. H., and Shin, Y. K. (1997) The membrane topology of the fusion peptide region of influenza hemagglutinin determined by spin-labeling EPR, *J. Mol. Biol. 267*, 1139−1148.
42. Rabenstein, M. D., and Shin, Y. K. (1995) Determination of the distance between two spin labels attached to a macromolecule, *Proc. Natl. Acad. Sci. U.S.A. 92*, 8239−8243.
43. Ottemann, K. M., Thorgeirsson, T. E., Kolodziej, A. F., Shin, Y. K., and Koshland, D. E. (1998) Direct measurement of small ligand-induced conformational changes in the aspartate chemoreceptor using EPR, *Biochemistry 37*, 7062−7069.
44. Yu, Y. G., Thorgeirsson, T. E., and Shin, Y. K. (1994) Topology of an amphiphilic mitochondrial signal sequence in the membrane-inserted state: a spin labeling study, *Biochemistry 33*, 14221−14226.
45. Laage, R., Rohde, J., Brosig, B., and Langosch, D. (2000) A conserved membrane-spanning amino acid motif drives homomeric and supports heteromeric assembly of presynaptic SNARE proteins, *J. Biol. Chem. 275*, 17481−17487.
46. Tokumaru, H., Umayahara, K., Pellegrini, L. L., Ishizuka, T., Saisu, H., Betz, H., Augustine, G. J., and Abe, T. (2001) SNARE complex oligomerization by synaphin/complexin is essential for synaptic vesicle exocytosis, *Cell 104*, 421−432
47. Rickman, C., Hu, K., Carroll, J., and Davletov, B. (2005) Self-assembly of SNARE fusion proteins into star-shaped oligomers, *Biochem. J. 388*, 75−79.

48. Han, X., Wang, C. T., Bai, J., Chapman, E. R., and Jackson, M. B. (2004) Transmembranesegments of syntaxin line the fusion pore of Ca2+-triggered exocytosis, *Science 304*, 289−292.
49. Hua, Y., and Scheller, R. H. (2001) Three SNARE complexes cooperate to mediate membrane fusion, *Proc. Natl. Acad. Sci. U.S.A. 98*, 8065−8070.
50. Danieli, T., Pelletier, S. L., Henis, Y. I., and White, J. M. (1996) Membrane fusion mediated by the influenza virus hemagglutinin requires the concerted action of at least three hemagglutinin trimers, *J. Cell Biol. 133*, 559−569.

BI052178+